PRODUCTION OF LINEARLY POLARISED PHOTONS

F. A. NATTER
Physikalisches Institut, Universität Tübingen, Tübingen, Germany

FOR THE PIP/TOF GROUP OF THE MAINZ A2 COLLABORATION

An improved modelling of bremsstrahlung production including collimation and experimental deficiencies are described as well as its realisation by two methods for calculating absolute and relative photon spectra and linear polarisation. Comparison of calculations and polarisation predictions with measured spectra are given, which indicate the precise (on a 2% level) and detailed description of the coherent and the incoherent contributions.

1 Introduction

Asymmetry measurements, which are especially sensitive on small amplitudes, provide an additional handle to the nuclear structure apart from cross section data. The use of linearly polarised photons as a tool in nuclear physics demands a reliable description of its production process and predictions of polarisation with small systematic uncertainties. The modelling of the bremsstrahlung spectra so far[1,2] seems not sufficient to describe different radiators and collimation angles with full consideration of all experimental deficiencies over a large energy range. Therefore several improvements were applied which allow to describe the absolute spectra as well as the relative ones to a high accuracy.

2 Kinematics and cross sections

Using energy and momentum conservation of the bremsstrahlung process a decomposition of the involved momenta with respect to the incident electron momentum in longitudinal q_l and transversal q_t components permits the formulation of kinematical limits for the momentum transfer $\vec{q}$:

$$\frac{\delta_x}{x} \geq q_l \geq \frac{q_t^2}{2E_0} + \delta_x \qquad \text{with} \quad \delta_x = \frac{x}{2E_0(1-x)} \tag{1}$$

This momentum transfer range, depending on the electron energy E_0 and relative photon energy $x = k/E_0$, is referred to as the 'pancake' due to its large lateral extension ($1 \gtrsim q_t \geq 0$). Calculating the bremsstrahlung cross section[3,4] but retaining the photon polarisation $\vec{\epsilon}$, the following asymptotic term is obtained: $\frac{d\sigma}{d\Omega} \propto \frac{1}{k}\cos^2\phi$. This shows that the cross section drops in first order with $1/k$ and that the maximal linear polarisation, with ϕ being the azimuthal angle of $\vec{\epsilon}$ with respect to the

scattering plane, is found in that plane. When employing an amorphous radiator, the electron scatters off a single atom which means that the momentum transfer $\vec{q}$ may lie at any point in the pancake leading to an isotropic distribution of $\vec{\epsilon}$, hence to an unpolarised beam. In contrast to this incoherent contribution an additional process can be observed in crystal radiators due to their regular structure: Whenever the momentum transfer coincides with a reciprocal lattice vector $\vec{q} = \vec{g}$ the recoil is absorbed by the whole lattice enhancing the yield by coherently adding the contributions of each atom. Also the momentum transfer is fixed in space which therefore leads to a polarised photon beam. Raising the photon energy x increases the coherent contribution and polarisation monotonically as well as q_l which depends like q_t on the orientation of the crystal $\Omega = (\theta, \alpha)$ (Fig. 2 and eq. A2) and leads to a discontinuity at $x_d = (1 + 1/(2E_0 g_l - g_t^2))^{-1}$, where a given lattice vector does not satisfy the pancake condition anymore and thus no longer contributes to the coherent bremsstrahlung spectrum. The total cross section of a crystal[5,6] is a sum of coherent and incoherent (including electron-electron) bremsstrahlung where the Debye-Waller factor $f_{\mathrm{Deb}}(q^2) \in [0, 1]$, which is a function of temperature and crystal properties, governs the fractioning into coherent and incoherent contributions to the total cross section. After introducing the intensity I per atom in units of $\bar{\sigma} = \alpha^2 Z^2 = 0.57947\ Z^2\mathrm{mb}$ the cross section and polarisation P are expressed as a sum over lattice vectors $\vec{g}$ of the functions $\Psi_{1,2,3}$ (eq. A1) and read in common notation:

$$I = \frac{x}{N\bar{\sigma}}\frac{d\sigma}{dx} = \left(1 + (1-x)^2\right)\Psi_1 - \frac{2}{3}(1-x)\Psi_2 \tag{2a}$$

$$P = 2(1-x)\Psi_3 \,/\, I^{\mathrm{cry}} = 2(1-x)\Psi_3 \,/\left(I^{\mathrm{coh}} + I^{\mathrm{inc}} + I^{\mathrm{e}}\right) \tag{2b}$$

In the coherent contribution due to kinematical constraints for a given lattice vector the photon polar angle $U = E_0 \vartheta_\gamma$ is a function of photon energy (eq. 3a), apart from a negligible dependence on the azimuthal angle[4]. Collimating the photon beam enhances the ratio of coherent to incoherent bremsstrahlung, thus increasing the degree of polarisation. Whereas the incoherent cross section is reduced approximately by $f_c = u_c/(1 + u_c)$ using a collimation angle of U_c (note: $u = U^2$), the coherent one stays unaffected in the energy range $x(\vec{g}\,) \in [x_c, x_d]$ but vanishes elsewhere:

$$U^2(x) = u(x) \approx \frac{g_l}{\delta_x} - \frac{g_t^2}{x} - 1 \tag{3a}$$

$$x_c = \left(1 + \frac{u_c + 1}{2E_0 g_l - g_t^2}\right)^{-1} = \frac{x_d}{1 + u_c(1 - x_d)} \tag{3b}$$

For the incoherent contribution instead of using the Bethe-Heitler cross section (eq. 3BSb in ref.[7]) the Hubbell[8] cross section derived from the Schiff cross section (eq. 3BSe), which has a more accurate dependence on photon energy, radiator charge

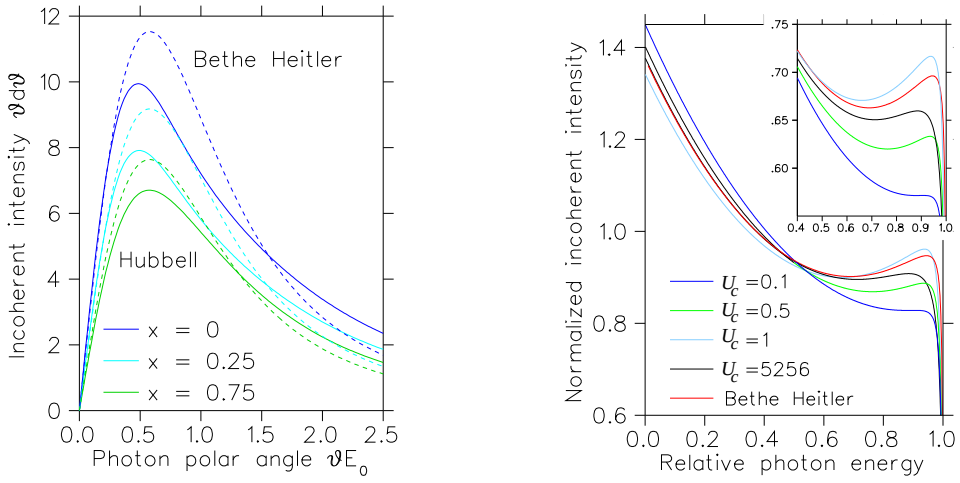

Fig. 1. Comparison of Z, photon energy and collimator angle U_c dependence of Bethe Heitler and Hubbell intensity. In the right panel the intensity was normalised to unity whereas in the insert the intensity was set to one at the origin ($I(0) = 1$) for the sake of comparison.

Z and collimation angle u_c was employed (see eq. A3 and Fig. 1). For a calculation of the incoherent contribution from a crystal radiator compared to an amorphous one, the Debye Waller factor $f_{\rm Deb}$ has to be taken into account, which leads to a modified form-factor: $(1 - F_{\rm Deb})^2 = (1 - f_{\rm Deb})(1 - F_r)^2$ denoted by $F_{\rm Deb}$. Here F_r means a realistic carbon form-factor from a Hartree Fock calculation[9]. Due to the fact that an analytical integration of the Schiff cross section as performed by Hubbell for the dipole form-factor with screening constant C (eq. A3) seems no longer feasible, two approximate treatments were investigated[4]. The use of an effective screening constant seemed superior because in addition the temperature dependence of $f_{\rm Deb}(T)$ is easier implemented there. The screening constant $C_{\rm eff}$ for the Hubbell cross section was determined via a fitting procedure for the total intensity $\int d\Gamma \sigma_{\rm BH}(1 - F_{\rm Deb})^2 = \int d\Gamma \sigma_{\rm Hub}(C_{\rm eff})$ with $d\Gamma = dx d\vartheta_\gamma d\vartheta_e d\phi_{e\gamma}$, resulting in $C_{\rm eff} = 91$ for the amorphous and 33 for the incoherent intensity.

Also an improved description[10] of the electron-electron bremsstrahlung I^e was used, which takes into account the binding energy of the radiator electrons and which has a non trivial Z and photon energy dependence, see (eq. A4). For this contribution the asymptotic Bethe-Heitler angular distribution $f(U) = U/(1 + U^2)^2$, which leads to the collimation reduction factor f_c (s. above) was adopted.

3 Treatment of experimental deficiencies

Up to now an ideal electron beam was assumed, but in experiments a deficient electron beam (Tab. 1) affects the photon spectra, especially the collimated ones. A finite beam spot size, characterised by the distribution w_{BS} of the impact positions

$\underline{s} = (s_x, s_y)$ of the electrons on the radiator, has the same effect like a collimator with a fuzzy edge and smears out the collimator cutoff in the photon spectra at x_c (eq. 3b). The primary divergence of the electron beam, described by the distribution w_{BD}, has a similar effect on x_c but causes in addition a variation of the crystal angles with respect to their nominal values Ω_0 changing the intensity due to the dependence of the momentum transfer on these angles. The deflection of the electron is not given by the beam divergence alone but is enhanced because the electron undergoes many small angle scattering processes mainly due to Coulomb interaction with atoms while traversing the radiator (thickness z_R). This distribution is well represented by Molières theory[11], which uses a Gaussian approximation for small angles defined by the variance $\sigma^m_{\text{plane}}(z)$ being a function of medium properties and pathlength z, the particle has travelled. The experimental photon intensity is a

Table 1. *experimental deficiencies and their influence on the photon spectra*

source	distr.	effect	influence
diamond temperature	-	Debye Waller factor	$I^{\text{coh}}/I^{\text{inc}}$
BS: beam spot size	$w_{BS}(\underline{s})$	"fuzzy" collimator	x_c
BD: beam divergence	$w_{BD}(\underline{p})$	+ variation of Ω_0	x_d
MS: multiple scattering	$w_{MS}(\underline{m})$	increases *BD*	x_d
ES: beam energy spread	$w_{ES}(p)$	smears out peaks	I^{coh}

sum over all these effects weighted with the appropriate distributions. Due to the collimation condition (a collimator with radius r_c is situated at distance z_c) the boundary of the integration volume in eq. 4 is topological non-trivial.

$$I_c^{\text{exp}} = \frac{1}{z_R}\int_R dz \int_{MS} d^2m \int_{ES} dE_0 \int_{BD} d^2p \int_{BS} d^2s \times w_{MS}(\underline{m}, z)\, w_{ES}(E_0)\, w_{BD}(\underline{p})\, w_{BS}(\underline{s})\, I^{\text{coh}}\big(\Omega_0, \underline{e}(\underline{p}, \underline{m})\big)\Big|_{r_c > |\underline{r}_\gamma(z_c, \underline{s})|} \quad (4)$$

Underlined vectors denote the transversal component of the respective unit vectors. This situation is sketched in Fig. 2 in order to clarify the relations used to calculate the experimental spectra via eq. 4. Two approaches will be presented: (ii) An accurate Monte Carlo method: MCB which permits the study of collimation effects on the photon beam and its polarisation in full dependence of all electron beam deficiencies[12]. (i) An analytical one: ANB which is approximative but very fast for quick first results.

3.1 Monte Carlo simulation: MCB

Measured electron beam parameters and their standard deviation as well as radiator and collimator properties are the basic input for calculations based on the

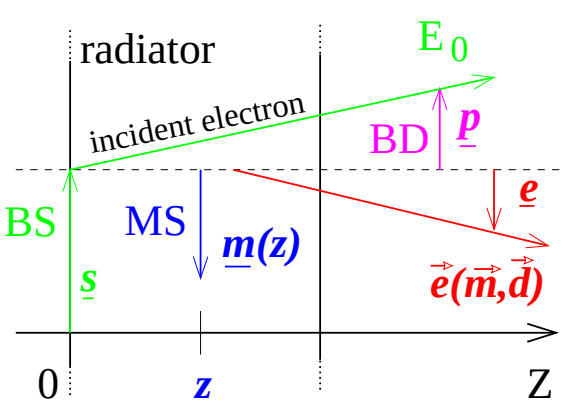

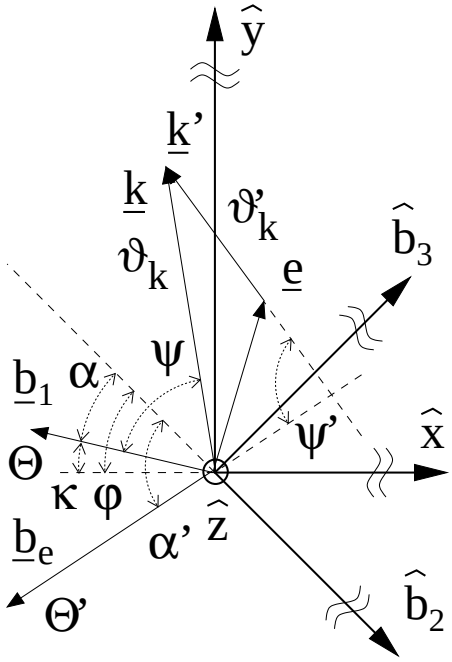

Fig. 2. (Left) Sketch of the momenta and vectors used in describing *BS*,*BD* and *MS* (see Tab. 1) and the resulting electron divergence (*ED*) vector $\underline{e}$. (Right) Angles and vectors, i.e. the reciprocal basis vectors $\underline{b}_i$, in reference to the lab system ($\hat{e}_i$). See also eqs. A5c and A2.

Monte Carlo technique. Starting from a given number of electrons N_e, depending on the desired statistical accuracy, a certain set of physical values are chosen randomly in parameter space. First the direction of an incident electron $\underline{p}$ with energy E_0 impinging at $\underline{s}$ on the radiator is chosen from the beam energy w_{ES} and divergence w_{BD} distributions, which are assumed to be of Gaussian shape with known parameters σ_{E_0}, $\sigma_p^{x,y}$ and $\sigma_s^{x,y}$ respectively. The mean polar angle deviation $\underline{m}(\sigma^m_{\text{plane}}(z))$ from the incident direction depend via Molières theory[11] on the depth z of the bremsstrahl process in the radiator, which is chosen randomly from a homogenous distribution within the radiator thickness z_R. To calculate the coherent bremsstrahlung for this particular electron the lattice has to be rotated into its coordinate system, involving a transformation of the crystal angles Ω_0. The total transversal electron deflection $\underline{e}$ due to multiple scattering and beam divergence and the transformation of the crystal $\hat{b}_1(\Omega_0)$ axis in the electron system $\hat{b}_e$ is calculated (eq. A5c and Fig. 2). Then a lattice vector is chosen uniformly in reciprocal space $V_{\vec{g}}$ with the Miller indices h, k, l, the intensity $I^{\text{coh}}(\vec{\Sigma})$ is calculated with these parameters $\vec{\Sigma} = (h, k, l, E_0, z, \underline{s}, \underline{m}, \underline{p}, \underline{k}, x)$ and the photon momentum $\underline{k}'$ is transformed back in the lab system. The resulting cross section is differential in photon energy k and angle, which is the azimuthal (ψ_k) in coherent bremsstrahlung and is the polar angle (ϑ_k) in the incoherent case. As an example the polarisation for a rectangular collimator compared to a circular one, both producing the same tagging efficiency, is shown in Fig. 3.

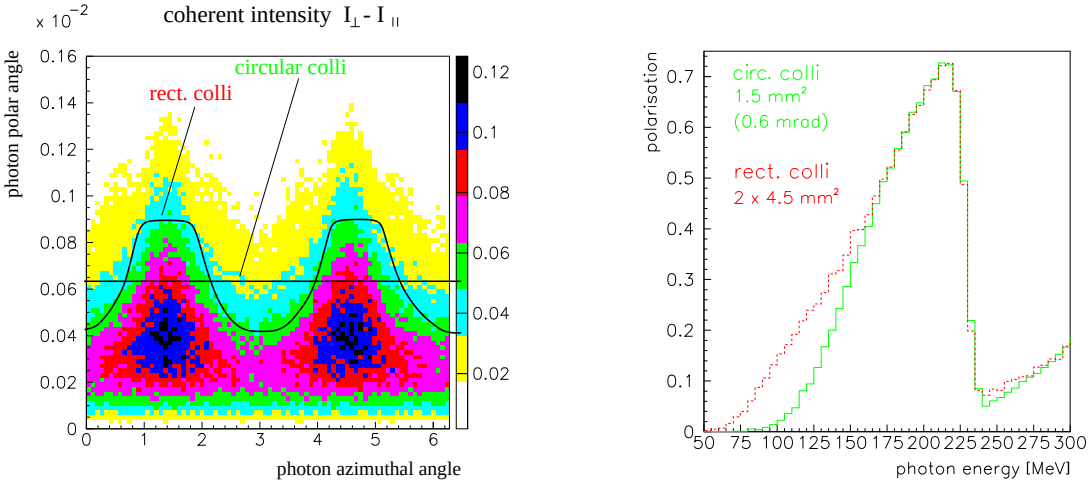

Fig. 3. Enhancement of polarisation at low energies (right) by use of a rectangular collimator instead of a circular one (left).

3.2 Analytical calculation: ANB

The following approximations were used to derive an analytical function from the complicated intensity expression (eq. 4): (i) All two dimensional transversal distributions are assumed to be Gaussian and approximated by azimuthal symmetrical Gaussian. (ii) A mean *MS* variance is used, averaged over the crystal. (iii) A combined total electron divergence (*ED*) distribution w_{ED} from a folding of the *MS* and *BD* distributions is used instead. (iv) The variation of g_t, being in second order of $\delta\Omega$ and therefore much smaller than the variation in g_l, is neglected in the intensity. With that the uncollimated coherent intensity (eq. 4) in terms of the variation l of g_l due to *ED* is expressed as follows:

$$I_{ED}^{\mathrm{coh}} \approx \int d^2e\; w_{ED}(\underline{e}) I^{\mathrm{coh}}\big(g_l(\underline{b}_e)\big) = \int_{g_l>\delta_x} dl\; w_l(l) I(l_0 + l) \qquad (5a)$$

$$\text{with} \quad w_l(l) = \frac{d}{dl}\int_{l>l(\underline{e})} d^2e\; w_{ED}(\underline{e}) \qquad \text{and} \quad g_l = l_0(\hat{b}_1) + l(\underline{e}) \qquad (5b)$$

The sole dependence of the intensity on l allows the conversion of the two dimensional integral to an integral over l in consideration of the kinematical constraint of the pancake. Eq. 5a has to be calculated numerically but for small *BD* ($\sigma_e \lessapprox 10^{-2}$) the integral may be solved analytically and will be presented in a forthcoming paper. A collimation function is derived in the following, which includes experimental deficiencies. In the electron coordinate system the circular collimator is characterised by a lateral displacement distribution $w_c(\delta r_c = \delta\rho z_c/E_0, \varphi_c)$ of its centre. Due to the azimuthal asymmetry, only the integral over the displacement $\delta\rho$ has to be calculated. The collimator angle is now a function of the displacement and

azimuthal photon angle $U(\rho, \phi)$, which results in a convolution of the intensity[4]:

$$I_c^{\mathrm{coh}} = \int \rho d\rho \, d\phi \, w_c(\rho) \int_0^{u(\rho,\phi)} du \, I_{ED}^{\mathrm{coh}}(x) \delta(u - u(x)) \tag{6}$$

Owing to the delta function the ϕ integration is trivial and the expression separates into the coherent intensity in terms of the Ψ_i functions and a collimation function $I_c^{\mathrm{coh}} = \sum_{\vec{g}} I_{ED}^{\mathrm{coh}}(x, \vec{g}) C(U(x))$. The treatment of collimation in the incoherent case works analogous, but the different angular dependence leads to a remaining integral (note: $v = 1/(1 + U_c^2)$:

$$I_c^{\mathrm{inc}} = \int dv \; c(v) I^{\mathrm{inc}}(v) \qquad \text{with} \quad c(v) = -\frac{1}{2v\sqrt{v - v^2}} \frac{dC(U)}{dU} \tag{7}$$

Therefore, a single collimation function accounts for experimental deficiencies in both cases of coherent and incoherent bremsstrahlung production. After these derivations, $C(U)$ and $c(v)$ have to be calculated numerically only once and the remaining evaluation of the intensities is a closed analytical calculation providing very fast results.

4 Results

Using the parameters from Tab. 2, intensities are calculated and are compared (Fig. 4) with measurements of the bremsstrahlung spectra for nickel and diamond radiators obtained at Mainz. The crystal angles were aligned such that the discontinuity of the $[02\bar{2}]$ lattice vector was located around 350 MeV. For the incoherent intensity (fig. 4a) the Hubbell cross section (eq. 7) was employed for nickel whereas the incoherent contribution for total crystal intensity in Fig. 4b stems from a calculation for carbon. Comparison of data and calculations on basis of absolute intensity are a more stringent test of the modelling then in terms of relative intensities $I^{\mathrm{rel}} = I^{\mathrm{coh}}/I^{\mathrm{Ni}}$, which are shown in Fig. 5. A check of the polarisation prediction is provided by a measurement of the beam asymmetry of coherent π^0 photoproduction[2]. The prediction is compared with the deduced photon polarisation and is in good agreement with the data for both collimation angles (Fig. 6).

5 Summary

The comparison of the data with the calculation indicates the high quality of the description. It can handle different radiators and collimators as well as the experimental deficiencies in its full complexity via the MC approach. The advantage of the approximative analytical treatment, which has a mean deviation of $\approx 3\%$ with respect to MCB, is its speed because it is about 500 times faster than MCB.

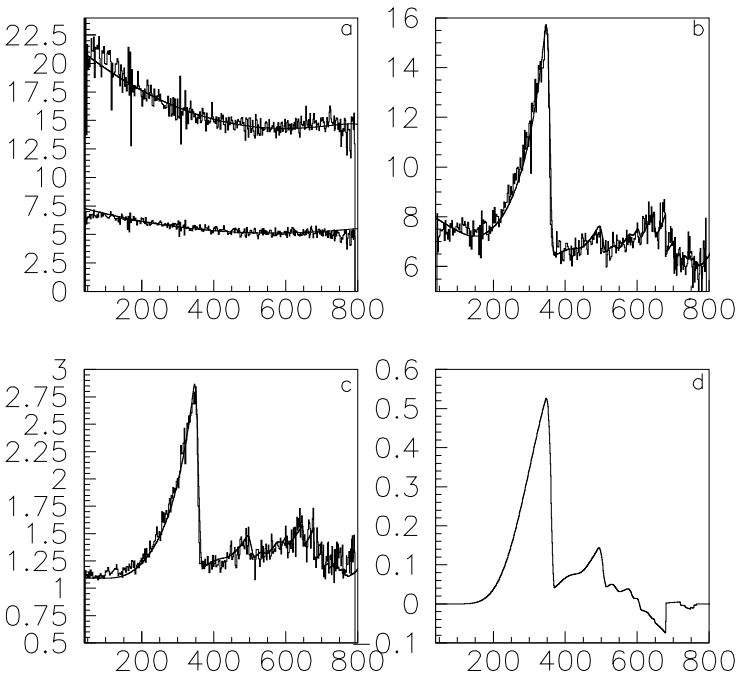

Fig. 4. Comparison of data and predictions for the absolut intensities: a) I^{Ni} with (top) and without (bottom) collimation, b) I^{cry}, c) relative intensity $I^{\mathrm{rel}} = \frac{I^{\mathrm{coh}}}{I^{\mathrm{Ni}}}$ and d) polarisation

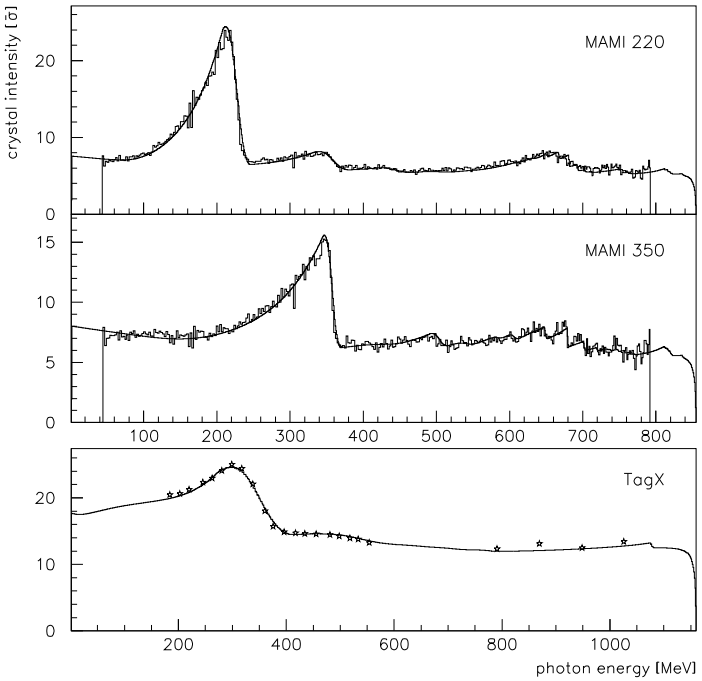

Fig. 5. Calculation of absolute crystal intensity $I^{\mathrm{cry}} = I^{\mathrm{coh}} + I^{\mathrm{inc}} + I^{e}$ compared to measurements of photon spectra at MAMI and TagX/Tokio (Tab. 2)

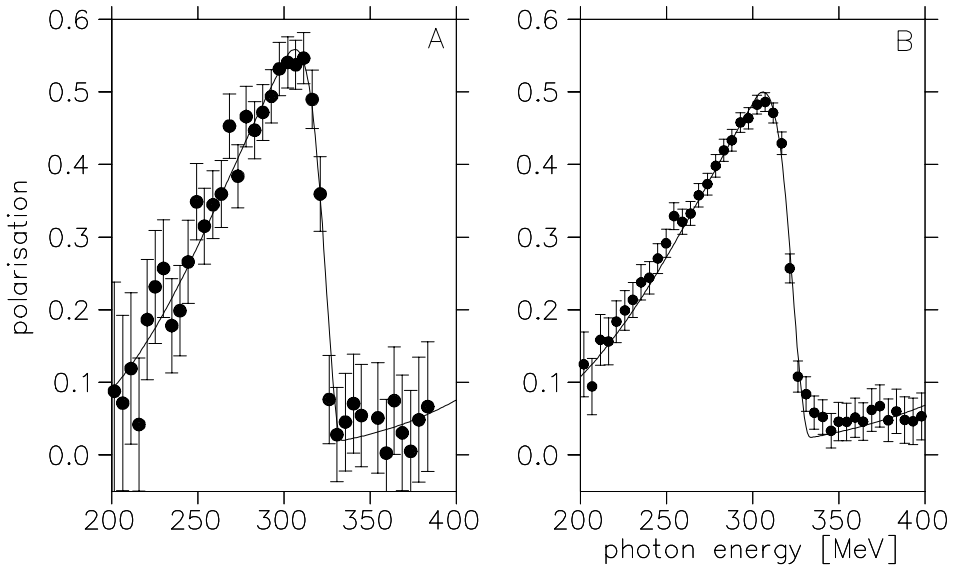

Fig. 6. Degree of linear polarisation from a calculation using the parameter of set A and B in comparison with a measurement of the asymmetry of coherent π^0 photoproduction [2].

With both codes photon spectra and polarisation prediction are reliably produced with a systematic error less than 2% adding only a small contribution from photon polarisation to the systematic error of asymmetries.

Acknowledgements

This work has been supported by grants from the DFG and DAAD.

References

1. D. Lohmann, M. Schumacher *et al.*, Nucl. Instrum. Methods **A343** (1994) 494,
   D. Lohmann, Diploma Thesis 1992, Georg-August-Universität Göttingen
2. F. Rambo, Diploma Thesis 1995, Georg-August-Universität Göttingen,
   F. Rambo, Phys. Rev. **C58** (1998) 489
3. W. Heitler, *The Quantum Theory of Radiation* (1954), Clarendon Press
4. F. A. Natter, PiPTOF internal report 99/1, Universität Tübingen
5. U. Timm, Fortschritte der Physik **17** (1969) 765
6. M. May, Phys. Rev. **84** (1951) 265
7. H.W. Koch and J.W. Motz, Rev. Mod. Phys. **31** (1959) 920
8. J.H. Hubbell, J. Appl. Phys., **30**, No. 7 (1959) 981
9. D.T. Cromer, J.T. Waber, Acta Cryst. **18** (1965) 104

10. J.L Matthews and R.O. Owens, Nucl. Instrum. Methods **111** (1973) 157
11. G. Molière, Z. Naturforschung **3a** (1948) 78
12. S. Wunderlich, Diploma Thesis 1998, Universität Tübingen

Appendix

Table 2. Parameters used for the calculation in Fig. 6. The diamond thickness and crystal angle was taken as $d = 0.1$ mm (1 mm for TagX) and $\Phi = \pi/4$, respectively.

set		θ	α	σ_{bspot}	σ_{bdiv}	ϑ_c
		[rad]	[rad]	[mm]	[mrad]	[mrad]
Fig. 4		.0607	.602	0.2	0.15	0.6
Fig. 6	A	.0607	.634	0.3	0.2	0.5
	B	.0607	.634	0.3	0.2	0.7
Fig. 5	220	.0607	.694	0.2	0.15	1.2
	350	.0607	.602	0.2	0.15	1.2
	TagX	.1501	.818	0.1	0.39	1.3

The coherent intensity expressed by means of the functions ψ_i^{coh} as derived in ref.[6] for an ideal electron beam without any experimental deficiencies read:

$$\Psi_1^{\mathrm{coh}} = 4\sum\nolimits_{\vec{g}} G\delta g_t^2 g_l^{-2} \qquad \Psi_2^{\mathrm{coh}} = 24\sum\nolimits_{\vec{g}} G\delta^2(g_l-\delta) g_t^2 g_l^{-4} \tag{A1a}$$

$$\Psi_3^{\mathrm{coh}} = -4\sum\nolimits_{\vec{g}} G\delta^3 g_l^{-4}\left[(g_2^2-g_3^2)\cos 2\phi + 2g_2g_3\sin 2\phi\right] \tag{A1b}$$

$$\text{and} \quad G(\vec{g}) = (2\pi)^2 a^{-3} S^2(\vec{g}) e^{-Ag^2} F^2(g^2) g^{-4}$$

Here, S and F are the crystal structure function and the atomic form-factor depending on the lattice vector $\vec{g}$, whereat the longitudinal and transversal momentum transfer entering the cross section in addition depend on the orientation of the crystal Ω:

$$g_l = g_1\cos\Theta + (g_2\cos\alpha + g_3\sin\alpha)\sin\Theta \tag{A2a}$$

$$g_t^2 = g_2^2 + g_3^2 + (g_1^2 - (g_2\cos\alpha + g_3\sin\alpha)^2)\sin^2\Theta \tag{A2b}$$

The incoherent collimated intensity functions $\psi_{\mathrm{coll},i}^{\mathrm{inc}}$, which result from an integration[8] of the Schiff cross section over the photon angle up to a collimator

angle U_c read in terms of $v = 1/(1+U_c^2)$:

$$\Psi_1 = 2\big[1 + M(1) - (1 + M(v))v - c\big] \tag{A3a}$$

$$\Psi_2 = -\frac{40}{3}v^3 + 18v^2 - \left(8\delta_z^2 + 6\right)v + 8\delta_z^2 + 2M(1) + \frac{4}{3} + \left(4v^3 - 6v^2\right)M(v) - 6\delta_z^2\left(M(v) - M(1) + \frac{2}{3}c\right) \tag{A3b}$$

$$\text{with} \quad M(v) = -\ln\left(\delta_z^2 + v^2\right) - 2\ln\frac{Z^{1/3}}{C}$$

$$c = 2\delta_z \arctan\left(\frac{1-v}{\delta_z + v/\delta_z}\right) \qquad \text{and} \quad \delta_z = \frac{C}{Z^{1/3}}\delta_x$$

The sophisticated treatment of the electron-electron bremsstrahlung by ref.[10] gives for the intensity functions ψ_i^e:

$$\Psi_1^e = \Psi_2^e - \frac{2}{3Z} = \frac{1}{Z}\left[\psi(\epsilon) - 4 - \frac{8}{3}\ln Z\right] \tag{A4a}$$

$$\psi(\epsilon) = \begin{cases} 19.9 - 4\ln\epsilon & \text{for } \epsilon \geq 0.88 \\ \sum_{n=0}^{5} e_n (0.88 - \epsilon)^n & \text{for } \epsilon < 0.88 \end{cases} \tag{A4b}$$

$$\text{with} \quad \epsilon = \frac{100}{E_0 Z^{2/3}}\frac{x}{1-x}$$

$$e_n = 19.7, 3.806, 31.84, 58.63, 40.77$$

The angles and vectors used here are related as follows, where in eq. A5a and A5b the vectors refer to the crystal ($\hat{b}_i$) and lab ($\hat{e}_i$) system respectively and in particular the reference for the transverse vectors is $\hat{b}_1$ or $\hat{z}$. Due to the smallness of θ transverse vectors ($\underline{t}$) differ in both systems negligible, for example: $\underline{t}|_{b_1} \approx \underline{t}$ or $\underline{b}_2 = \hat{b}_2 - (\hat{b}_2\hat{z})\hat{z} \approx \hat{b}_2$:

$$\kappa = \angle(\underline{e}_x, \underline{z}) \qquad \alpha = \angle(\underline{z}, \hat{b}_2) \qquad \phi = \angle(\underline{e}_x, \hat{b}_2) \tag{A5a}$$

$$\kappa = \angle(\hat{e}_x, -\underline{b}_1) = \phi - \alpha \qquad \alpha = \angle(-\underline{b}_1, \hat{b}_2) \qquad \phi = \angle(\hat{e}_x, \underline{b}_2) \tag{A5b}$$

$$\underline{b}_1(\Omega_0) = \theta_0(-\cos\kappa, \sin\kappa) \qquad \underline{b}_e = \underline{b}_1 - \underline{e} \tag{A5c}$$